


Article

Theoretical and Experimental Investigations into Novel Oxynitride Discovery in the GaN-TiO₂ System at High Pressure

Alwin James ^{1,*} , M. Mahdi Davari Esfahani ^{2,3,*}, William R. Woerner ², Alexandra Sinclair ⁴, Lars Ehm ^{2,4}, Artem R. Oganov ^{2,5,6,7} and John B. Parise ^{1,2,4}

¹ Department of Chemistry, State University of New York, Stony Brook, NY 11794, USA;

john.parise@stonybrook.edu

² Department of Geosciences, State University of New York, Stony Brook, NY 11794, USA;

wwoerner@eag.com (W.R.W.); lars.ehm@stonybrook.edu (L.E.); artem.oganov@stonybrook.edu (A.R.O.)

³ Center for Materials by Design, Institute for Advanced Computational Science, State University of New York, Stony Brook, NY 11794, USA

⁴ Mineral Physics Institute, Stony Brook University, Stony Brook, New York 11794, USA; magneticfrustration@gmail.com

⁵ Skolkovo Institute of Science and Technology, Skolkovo Innovation Center, 3 Nobel Street, Moscow 143026, Russia

⁶ Department of Problems of Physics and Energetics, Moscow Institute of Physics and Technology,

9 Institutskiy Lane, Dolgoprudny City, Moscow 141700, Russia

⁷ International Center for Materials Design, Northwestern Polytechnical University, Xi'an 710072, China

* Correspondence: alwin.james@stonybrook.edu (A.J.); mahdi.davari@stonybrook.edu (M.M.D.E.)

Received: 31 December 2017; Accepted: 19 January 2018; Published: 23 January 2018

Abstract: We employed ab initio evolutionary algorithm USPEX to speed up the discovery of a novel oxynitride in the binary system of GaN-TiO₂ using high-pressure synthesis. A 1:2 mixture of GaN and nanocrystalline TiO₂ (anatase) was reacted under 1 GPa of pressure and at 1200 °C in a piston cylinder apparatus to produce a mixture of TiO₂ (rutile) and an unknown phase. From the initial analysis of high resolution neutron and X-ray diffraction data, it is isomorphic with monoclinic V₂GaO₅ with a unit cell composition of Ga₁₀Ti₈O₂₈N₂ with the following parameters: monoclinic, space group C2/*m*, *a* = 17.823(1) Å, *b* = 2.9970(1) Å, *c* = 9.4205(5) Å, β = 98.446(3)°; Volume = 497.74(3) Å³. Further, a joint rietveld refinement revealed two distinct regimes—A Ti-rich block and a Ga-rich block. The Ti-rich block consists of four edge-shared octahedra and contains a site which is about 60% occupied by N; this site is bonded to four Ti. The remainder of the block consists of edge linked Ti-octahedral chains linked to the TiN/TiO fragments at octahedral corners partially occupied by nitrogen. The Ga-block contains two symmetry independent octahedral sites, occupied mostly by Ga, and a pure Ga-centered tetrahedral site bonded mostly to oxygen.

Keywords: oxynitrides; water splitting; high pressure; crystal structure prediction; USPEX

1. Introduction

The search for alternatives to fossil fuels is driven by increasing energy demands, and the desirability of limiting growth in CO₂ in the atmosphere, while retaining the advantages of fuel transportability. In this regard, visible light [1] driven photocatalysis for overall water splitting (OWS) might produce chemical fuels, such as hydrogen, which would address these criteria [2,3].

Traditional OWS photocatalysts, such as titanium dioxide (rutile) are inorganic oxides with large bandgaps and activity only under ultraviolet light. Rutile is a photosensitizer capable of oxidized organic dyes [4], and it was identified as a photocatalyst in 1956 by Mashio et al. [4]. Water splitting was observed with TiO₂ a photo-anode and platinum cathode and an external bias in the pioneering

work of Honda and Fujishima et al. [5,6]. Other oxides identified as capable of OWS include SrTiO_3 perovskite and $\text{K}_2\text{La}_2\text{Ti}_3\text{O}_{10}$, a Ruddlesden–Popper phase [7].

Oxynitrides and solid solutions containing nitrogen absorb the majority of solar spectrum [8–11] compared to the traditional inorganic oxide photocatalysts due to their higher N2p valence states and smaller bandgaps. For example, LaTiO_2N , produced by the ammonolysis of $\text{La}_2\text{Ti}_2\text{O}_7$, absorbs visible light [12,13]. Attempts to introduce nitrogen into Ti based photocatalysts had varied success. Bimetallic oxynitride perovskites, which contain titanium, are common [10,14] while pure titanium oxynitride compounds exist rarely; sometimes as thin films [15,16].

An important recent discovery was a GaN rich solid solution $(\text{GaN})_x(\text{ZnO})_{1-x}$, reported by Domen et al. [8,17]. Members of the solid solution have bandgaps smaller than the GaN and ZnO endmembers. In addition, they achieved overall water splitting at relatively high efficiency of up to 6%. Inspired by these results, we synthesized the complete solid solution $(\text{GaN})_x(\text{ZnO})_{1-x}$ under pressure and demonstrated hydrogen evolution from water without the use of cocatalysts and sacrificial reagents [18]. Further, we investigated the possibility of other oxynitride solid solutions that might go beyond currently available efficiencies. We selected GaN– TiO_2 , cognizant of arguments that d^0 and d^{10} oxynitrides are likely to lead to OWS catalysts [8]. While it is desirable to produce an OWS catalyst at near ambient pressure, our previous high pressure work suggested high pressure synthesis allows for better control over stoichiometry, which is not always available from ammonolysis. Further, recent computational search based on published databases [19] suggests that many novel oxynitrides have high instability indices at ambient pressure, and that high pressure followed by quench recovery may be required for their synthesis. High pressure experiments are difficult, requiring multiple runs for their optimization, and our previous work on Nb_2O_5 –GaN system [20] used crystal structure prediction methods and in situ high resolution X-ray scattering to mitigate this disadvantage. Here, using state of the art evolutionary algorithm USPEX along with density functional theory calculations, we studied the pressure-driven stability of GaN– TiO_2 system to better understand and evaluate the structures and stability fields of possible Ga–Ti–oxynitride compounds with chemical composition chosen from a mix of GaN and TiO_2 endmembers.

2. Results

2.1. Theoretical Predictions Using USPEX

We constructed the convex hull, which connects the phases that are stable against decomposition into elements or binaries at a given pressure. The convex hulls were obtained from the enthalpies of the most stable structures of compounds at a given pressure. The enthalpy of formation of the lowest enthalpy Ga–Ti–oxynitrides at 0, 5, 10 and 20 GPa are given in Table 1, which simply shows a tendency for structures with 1:1 and 1:2 ratios of GaN: TiO_2 to move to lower formation enthalpy with increasing pressure. This trend suggests their potential stability with increasing pressure.

Table 1. Enthalpies of formation of GaTiO_2N and $\text{GaTi}_2\text{O}_4\text{N}$ calculated at 0, 5, 10 and 20 GPa.

Pressure	Formation Enthalpy (eV/atom)	
	GaTiO_2N	$\text{GaTi}_2\text{O}_4\text{N}$
0 GPa	0.19	0.21
5 GPa	0.14	0.15
10 GPa	0.13	0.14
20 GPa	0.10	0.11

The structures of the predicted ordered GaTiO_2N and $\text{GaTi}_2\text{O}_4\text{N}$ phases are illustrated in Figure 1 and the Crystallographic Information Files (CIF) are described in the appendix (Table A2). Although not all structural aspects of these ordered phases did match with the disordered experimental

phase described in Section 2.2, ab initio calculations at 0 K provided a useful guide to target compositions that are within thermodynamically synthesizable range.

Analysis of X-ray and neutron scattering data suggests that the experimentally synthesized new phase has the composition of $\text{Ga}_{10}\text{Ti}_8\text{O}_{28}\text{N}_2$. After obtaining this result, we performed phase stability calculations for $\text{Ga}_{10}\text{Ti}_8\text{O}_{28}\text{N}_2$ against the decomposition to oxynitrides and oxide endmembers i.e., $\text{Ti}_3\text{O}_3\text{N}_2$ and Ga_2TiO_5 , however, the decomposition reaction energies indicate that $\text{Ga}_{10}\text{Ti}_8\text{O}_{28}\text{N}_2$ is an entropy-stabilized oxynitride. The decomposition reaction energies are obtained as follow: 15 meV/atom at 10 GPa and 4 meV/atom at 20 GPa, which indicates its stability with increasing pressure.

Entropy can have a significant impact on free energy calculations of disordered structures; however, incorporating entropy is computationally expensive. Entropy is a sum of the electronic entropy (S_{el}), configurational entropy (S_{conf}) and vibrational entropy [21]. The electronic entropy S_{el} is easy to calculate, but does not have a significant effect on the free energy. On the other hand, vibrational S_{vib} and configurational S_{conf} entropies are very expensive and can have significant effect on free energy. The configurational entropies are calculated based on Boltzmann's formula which relates entropy values to the number of the accessible arrangement of atoms in the lattice [22].

$$S_{conf} = k \ln g(\sigma), \quad (1)$$

where k is the Boltzmann constant and $g(\sigma)$ is the number of all possible configurations. The general formula for the configurational entropy can be obtained from:

$$S_{conf} = -k \sum (P_j \ln P_j + (1 - P_j) \ln (1 - P_j)), \quad (2)$$

where P_j is the probability of a certain configuration j . Configurational entropies are calculated based on the above formula and the stabilizing temperatures are calculated from:

$$T = \frac{\Delta H_{ordered-disordered}}{\Delta S} \quad (3)$$

where $\Delta H_{ordered-disordered}$ is the difference between enthalpies of ordered and disordered structures and $\Delta S = S_{conf}$. Configurational entropies and required temperatures for stabilizing GaTiO_2N , $\text{GaTi}_2\text{O}_4\text{N}$ and $\text{Ga}_{10}\text{Ti}_8\text{O}_{28}\text{N}_2$ are listed in Table 2. The experimentally-observed mixed tetrahedral and octahedral coordination of Ga is accurately predicted with USPEX; however, Ti is predicted to exist in a mixture of octahedral and heptahedral coordination while experiments only observe octahedral Ti. In addition, bond valences are calculated according to $S_i = \sum_j \exp[(R_0 - R_{ij})/B]$, where B is 0.37 and R_0 is obtained from published tables [23]. Bond valences for Ga and Ti of the predicted structures are consistent with the experimental phase.

Table 2. Configurational entropies and calculated temperatures needed to stabilize given compounds.

Compound	S_{conf} (eV K ⁻¹ /F.U.)	T (K)
GaTiO_2N	3.29	1408
$\text{GaTi}_2\text{O}_4\text{N}$	4.41	1684
$\text{Ga}_{10}\text{Ti}_8\text{O}_{28}\text{N}_2$	6.38	3494

Theoretical and experimental structural studies revealed that the synthesized phase has positional disorder among both the cations and the anions sites. Since oxygen and nitrogen have similar ionic size, electronegativities and coordination number, these anions are usually disordered across anion sites [9], and hence makes it a real challenge for crystal structure prediction methods. Partial ordering have been observed in some oxynitrides [24–26], however, ideally ordered oxynitrides are scarce between known oxynitrides e.g., TaON and $\text{Si}_2\text{N}_2\text{O}$ [27,28]. While incorporating disorder is not

practical with crystal structure prediction methods at the current stage of development, the predicted structures give insights into the chemistry of the system, may guide experimental efforts, and contain structural features, such as the separation of Ti and Ga into different structural blocks, which is confirmed in the experimental analysis. In addition, the average bond lengths of the predicted phases, (Figure 1 & Table A3) are in a good agreement with the experimental data.

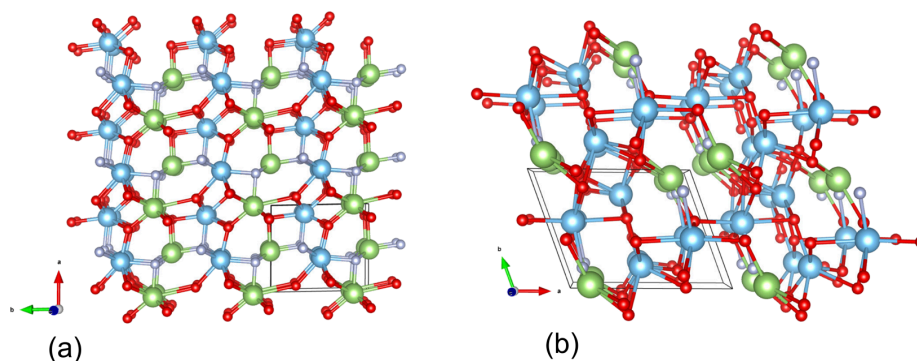


Figure 1. The lowest enthalpy structures of (a) GaTiO₂N and (b) GaTi₂O₄N predicted at 20 GPa. Green and blue spheres are gallium and titanium atoms, respectively. Oxygen and nitrogen are represented by red and silver spheres, respectively. The unit cells are outlined with black lines. Visualization is done by VESTA [29].

2.2. Crystallographic Characterization

In anticipation of the inability of X-rays to distinguish between O and N in the anion sites, and because of the favorable scattering contrast between Ga and Ti, $b_N = 7.29$ fm and -3.44 fm, respectively, initially only neutron diffraction data, collected on the POWGEN instrument at the Spallation Neutron Source at Oak Ridge National Laboratory, TN, were utilized. Unit cell indexing and structure solution identified the new phase designated presumptively as “Ga-Ti-O-N”, is isomorphic with monoclinic V₂GaO₅, $C2/m$, $Z = 6$, $a = 17.758(5)$ Å, $b = 2.990(1)$ Å, $c = 9.323(3)$ Å and $\beta = 98.44(2)^\circ$ [30]. From the crystal structure of V₂GaO₅ we can construct a solid solution that accounts for the coupled substitution of Ti/N into the full unit cell contents ($Z = 6$) of V₁₂Ga₆O₃₀. The oxide and oxynitride endmembers of this solid solution would then be Ga₁₂Ti₆O₃₀ and Ti₁₈O₁₈N₁₂, respectively. More generally, the solid solution is formulated as Ti_{6+x}Ga_{12-x}O_{30-x}N_x; empirical formula Ti_{1+x}Ga_{2-x}O_{5-x}N_x. This formulation provided chemical constraints utilized in the latter stages of structure refinement.

An X-ray diffraction pattern was collected on the high resolution powder [31,32] instrument at beamline 11-BM at the Advanced Photon Source, IL, by taking advantage of the mail-in service at this facility [33]. The X-ray data provides an independent means of determining the Ga/Ti content; this is particularly important since the presumed unknown phase designated isomorphous to V₂GaO₅ phase is nonstoichiometric [30]. Any sample related variables, such as residual strain, can also be best determined from the high angular resolution X-ray data. Further, the small size of the sample, its multiphase nature, and the relative complexity of the Ga-Ti-O-N phase, is well matched to the high angular resolution at the 11-BM instrument. The initial X-ray refinements were constrained by assuming a pure oxide composition, Ga and Ti distributed randomly over all cation sites consistent with the presumed chemistry derived from V₂GaO₅, that is Ga₂TiO₅, and with displacement parameters for all atoms fixed to a common value ($U_{iso} = 0.01 \text{ \AA}^2$). The peak width parameters were fixed to values determined from a LaB₆ standard, which also provided the X-ray wavelength, $0.412447(5)$ Å. The sample on which X-ray data were collected was identical to the one used for neutron-data collection. Because of the superior counting statistics (Figures 2 and 3) a small amount of an unidentified phase was obvious in the XRD pattern. The largest peaks from this phase were around 7.2 , 7.5 , 9.3 , and 14.2° in 2θ and the most intense peak of the unindexed phase match that of rutile

and Ga-Ti-O-N phases; the amounts were estimated to be 1% and 2% of those phases, respectively. Those regions containing peaks from the unidentified phase were excluded from refinements utilizing the X-ray data. These peaks were not observed in the neutron data, probably because of insufficient peak-to-background discrimination.

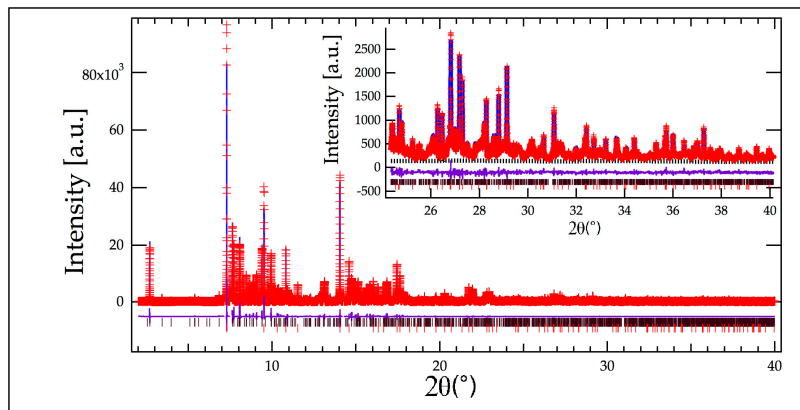


Figure 2. Fit to X-ray data; observed and calculated data are red crosses and the continuous blue line, respectively. The dotted and solid black curves represent the background and the difference between observed and calculated data, respectively.

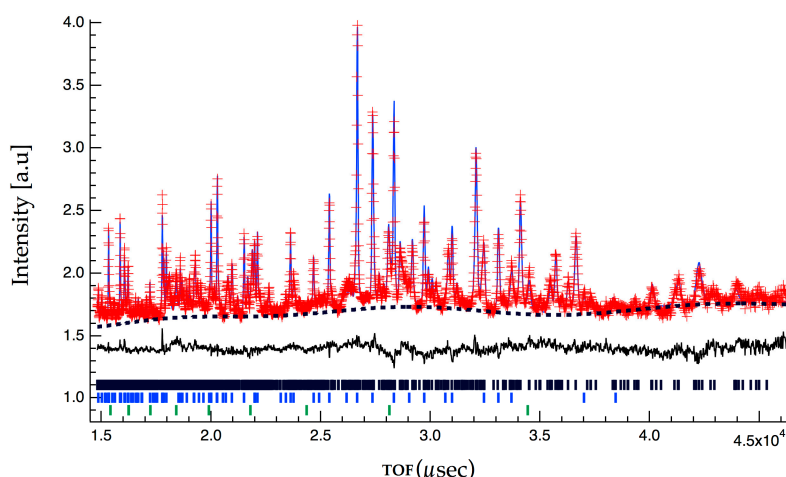


Figure 3. Fit to neutron data; observed and calculated data are red crosses and the continuous blue line, respectively. The dotted and solid black curves represent the background and the difference between observed and calculated data, respectively. The vertical black, blue and green lines mark the positions of Bragg reflections from the Ga-Ti-O-N, TiO₂ (rutile) and vanadium sample can, respectively. The largest differences between observed and calculated data are in the rutile phase.

Refinement began with background parameters (cosine series, 12 parameters) and scale factor. Following convergence, cell parameters for both rutile and Ga-Ti-O-N phases were added to the refinement. The differences between observed and calculated patterns was dominated by anisotropic broadening of the Ga-Ti-O-N phase. Refinement of a generalized anisotropic broadening model [34,35] for Ga-Ti-O-N, improved the fit considerably as shown in Figure 2, which is a smaller region of the fit.

The question of stoichiometry was addressed by refining positional parameters, followed by refinement of all metal site occupancies with fixed displacement parameters for all atoms ($U_{\text{iso}} = 0.005 \text{ \AA}^2$), the total occupancy of anion sites fixed to one oxygen, and metal sites constrained to be fully occupied. These assumptions were tested further in joint X-ray-neutron refinements discussed below. At this stage, refinement using just the X-ray data suggested some cation sites were partially

disordered but that all were preferred by either Ga or Ti, or indeed were fully occupied by one or other of these metals. For example, the tetrahedral site (Figure 3) is occupied exclusively by Ga, while the block of sites at $x = 0$ and $x = \frac{1}{2}$ are essentially pure Ti, with about 20% Ga-substitution in the remaining TiGa sites (Figure 3). The refined Ga/Ti ratio was approximately 1.25, which would correspond to a unit cell composition of $\text{Ga}_{10}\text{Ti}_8\text{O}_{28}\text{N}_2$.

A joint refinement utilizing both X-ray and neutron data was then initiated. The strain parameters for rutile and Ga-Ti-O-N were refined independently (Figure 4) but constrained to be equal for each phase between X-ray and neutron datasets. The neutron data was weighted at 1.5, compared to the X-ray data weighted at 1.0, to emphasize the favorable scattering differences between O/N and Ga/Ti pairs occupying anion and cation sites, respectively. Starting with the unit cell composition consistent with refinement of cation site occupancies from the X-ray data, $\text{Ga}_{10}\text{Ti}_8\text{O}_{28}\text{N}_2$, atoms were distributed randomly over the cation and anion sites. The neutron refinement was initiated by sequentially refining overall parameters, background and scale, for individual data sets, and then sample parameters common to both datasets, strain and unit cell dimensions. To account for slight differences arising due to the temperatures at which neutron data were collected, elastic strain components were refined for both phases for the X-ray data set. The neutron dataset was contaminated by peaks arising from the vanadium sample holder, and this phase was added to account for this. Following convergence of a refinement of the above parameters and the site positional parameters for the Ga-Ti-O-N phase, the anion and cation site occupancies were determined.

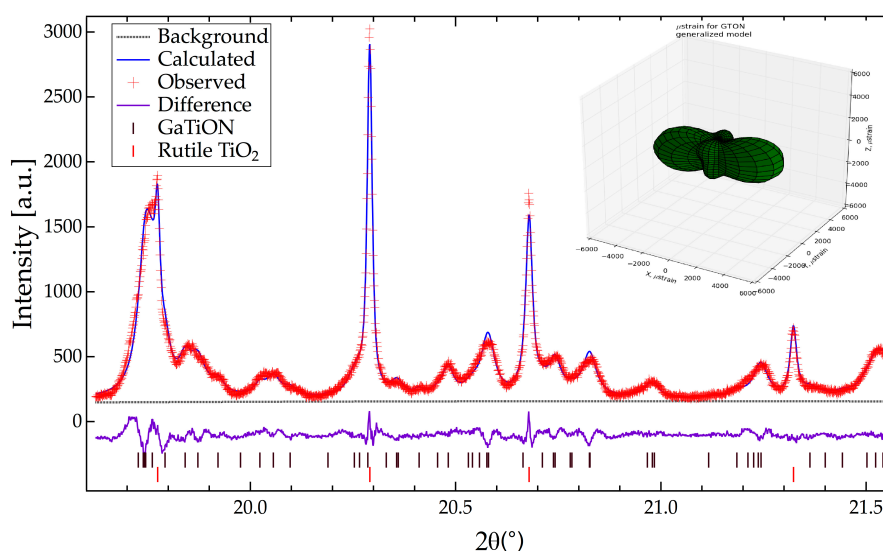


Figure 4. Rietveld fit to 11-BM (APS) X-ray profile containing an estimated TiO_2 (46 wt %) and the new phase related to V_2GaO_5 (54 wt %). Note the much larger anisotropic strain, defined in GSAS-II [34] and originally introduced [35] and used by Stephens [36,37]. Note the sharper rutile peaks (vertical red markers) compared to those of the V_2GaO_5 -related phase (vertical black markers).

To set a baseline for comparison of the overall fit, all anion sites were filled with oxygen while the Ga-Ti occupancies of cation sites were refined along with overall displacement parameters (U); the value of U for all cation sites were constrained to be equal, as were those of the anion sites. The results of this refinement suggested the following approximate compositions for the five cation sites (see Table A1, which summarizes the final results for Ga-Ti-O-N): site 1, $\text{Ga}_{\frac{3}{4}}\text{Ti}_{\frac{1}{4}}$; site 2, Ti; site 3, $\text{Ga}_{0.8}\text{Ti}_{0.2}$; site 4, Ti; site 5, Ga. The fit to the neutron data, summarized by the weighted profile R-value (R_{wp}) and goodness of fit (GOF) were 5.81% and 3.70, respectively. The fits to the Ga-Ti-O-N phase Bragg intensities, $R_B(F^2)$, comparable to the usual single crystal discrepancy factor, were 5.27% and 12.86%, for the X-ray and neutron data, respectively. The site occupancies of all metal and anion sites were then varied, with U_{iso} constrained as above. The results of this refinement were: neutron overall

$R_{wp} = 5.34\%$, $GOF = 3.64$, and $R_B(F^2) = 5.25\%$ and 10.14% , for the X-ray and neutron data, respectively. Sites that were within the margin of error of full occupancy by Ga, Ti and O were fixed at those compositions; no anion site was fully occupied by nitrogen. A new set of refinements was performed, maintaining restraints on strain and displacement parameters as described above. Trial refinements with displacement parameters refined without constraint did not significantly improve the overall fit. Finally, the chemical composition was constrained to be consistent with the formula derived for the solid solution $Ti_{6+x}Ga_{12-x}O_{30-x}N_x$; the amount of nitrogen per unit cell distributed over sites occupied by both oxygen and nitrogen, designated as “ON” sites ON1, 2, 4 and 8, was set equal to the amount of titanium in sites GaTi1 and 3 (Table A1). After convergence, the results summarized in Table A1 were obtained. The overall fits to the X-ray and neutron data are given in Figures 2 and 3, respectively. The CIF file for the experimental phase is deposited into Crystallography Open Database (COD entry 3000168) as prepublication data.

3. Discussion

3.1. Composition

The unit cell contents for the synthesized Ga-Ti-O-N phase were $Ga_{10}Ti_8O_{28}N_2$, consistent with the solid solution between theoretical endmembers $Ti_{18}O_{18}N_{12}$ and $Ti_6Ga_{12}O_{30}$, $Ti_{6+x}Ga_{12-x}O_{30-x}N_x$. The sites occupied by nitrogen tend to be segregated into those anion sites associated with the pure Ti-octahedral sites in blocks of structure centered at $x = 0, \frac{1}{2}$ (Figure 5, Table A1). If all ON sites were fully occupied by nitrogen this would correspond to N_{14} per unit cell, more nitrogen rich than the endmember composition, and so probably a composition that would not crystallize in this structure type. Interestingly, the presumptive pure Ti endmember composition, $Ti_{18}O_{18}N_{12}$ or $Ti_3O_3N_2$, is one predicted to have ideal bandgap properties for overall water splitting [19] albeit with a predicted instability of 31 meV per atom [19] that probably requires high pressure for synthesis. Wu et al.’s prediction is based upon Ti/O coupled substitution into the Ta_3N_5 structure [19]. The structure of Ta_3N_5 is orthorhombic $Cmcm$, $a = 3.8862 \text{ \AA}$, $b = 10.2118 \text{ \AA}$, $c = 10.2624 \text{ \AA}$ and consists of only distorted TaN_6 octahedra [38]. The Ta_3N_5 structure [38] is very different from that of $Ga_{10}Ti_8O_{28}N_2$ reported here (Figures 3 and 4). It would be interesting to attempt the synthesis of the titanium endmember “ $Ti_3O_3N_2$ ”. Our preliminary attempts to do so using ammonolysis of TiO_2 were not successful.

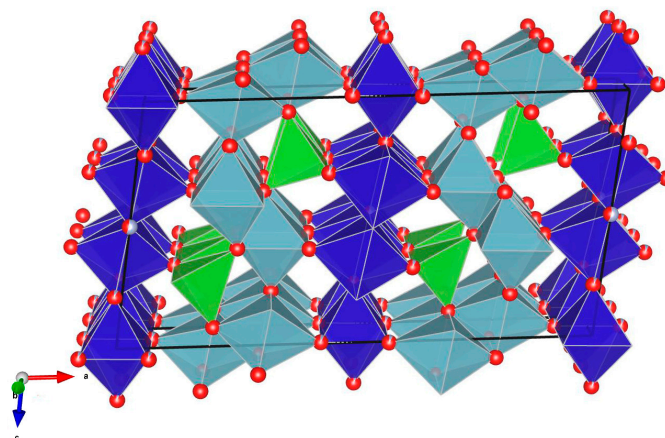


Figure 5. Structure of Ga-Ti-O-N, the gallium titanium oxynitride phase. Visualization is done by VESTA [29]. Deep blue polyhedra are occupied exclusively by Ti sites, green pure Ga and light blue are mixed Ti/Ga sites. Red balls represent anion sites occupied by oxygen; ON sites occupied mostly by nitrogen and by ~10% nitrogen, are represented by partially red and grey balls. The origin of the unit cell centered on Ti and is in the back top-left-hand corner, with z vertical, x to the right and y out of the page. The sites occupied by nitrogen are separated mostly into sites within blocks of Ti-centered octahedra, while oxide sites occupy mostly blocks occupied by Ga- and mixed TiGa sites.

3.2. Implications and Future Work

It is evident that state of the art evolutionary algorithm USPEX can be used reliably to find high pressure phases of oxynitrides with enough structural details and that will be utilized to explore several other oxynitride systems. In fact, the results obtained here will act as a feedback to assist us. We are continuing the synthesis work at even higher pressures in a multianvil press to find out if we can synthesize other members of the solid solution. Further, we are developing methods to predict materials with desired bandgaps more efficiently.

4. Materials and Methods

4.1. Theoretical Prediction Methods

Ab initio variable-composition evolutionary algorithm USPEX [39–43], which simultaneously searches for stable stoichiometries and their corresponding most stable structures, was employed to search for stable oxynitrides at pressures attainable in a large volume press. In this method, all stoichiometric compounds are considered following a constraint on the total number of atoms on the unit cell. We performed calculations at 0, 5, 10 and 20 GPa for systems having up to 48 atoms in the unit cell. Using USPEX, we generate stoichiometric compounds with initial chemical composition randomly chosen from a mix of GaN and TiO₂ and their corresponding structures generated using random symmetric generator. USPEX makes subsequent generations with 20% random structures, and 80% using heredity, soft-mutation, lattice mutation and transmutation operators, in which transmutation and heredity operators change the composition, while lattice mutation and soft-mutation only change the structure within a fixed-composition mechanism. After relaxing the structures, only the best 60% of the structures, ranked by a fitness function, are used to generate the subsequent generations.

The underlying structure relaxation was carried out using the all electron projector-augmented wave (PAW) method [44] as implemented in the VASP package [45] in the framework of DFT. We used valence electron configurations of [3p⁶ 3d² 4s²], [4s² 4p¹], [2s² 2p⁴] and [2s² 2p³] for titanium, gallium, oxygen and nitrogen, respectively. We used Perdew-Burke-Ernzerhof generalized gradient approximation (PBE-GGA) [46]. A plane-wave kinetic cutoff energy of 600 eV and dense Monkhorst-Pack k-points grids with reciprocal space resolution $2\pi \times 0.05 \text{ \AA}^{-1}$ were employed [47] in order to provide sufficient accuracy during enthalpy calculations.

4.2. High Pressure Synthesis

A 1:1 mixture of GaN, produced from the ammonolysis of powdered Ga₂O₃ (Alfa Aesar, Thermo Fisher Scientific Chemicals Inc., Ward Hill, MA, USA, 99.99%) and TiO₂ (Aldrich, Sigma-Aldrich, Saint Louis, MO, USA, 99.8% trace metals basis, anatase) was mixed thoroughly for half an hour in a mortar and pestle. About 1 g of this mixture was loaded into a piston-cylinder apparatus with a 19 mm diameter cylindrical talc pressure cell and rapidly heated at $\sim 200 \text{ }^\circ\text{C min}^{-1}$ to 1200 $^\circ\text{C}$, at 1 GPa. Details of this instrument was described in the literature [20]. The pressure and temperature was selected based on the previous research experience, where we saw that disorder in a system can bring about the stabilization of high pressure phases at even lower pressures than expected [20]. A mixture of TiO₂ (rutile) and an unknown phase resulted after the reaction. In an attempt to increase the yield of the unknown phase, the reaction mixture was adjusted to TiO₂:GaN = 2:1, and a nano form of the TiO₂ polymorph anatase (Nanostructured & Amorphous Materials, Inc., Houston, TX, USA, 99.4%) was used as a reactant along with crystalline GaN. About 50% of the anatase reacted with GaN before converting to the more refractory rutile polymorph. This sample, containing rutile and Ga-Ti-O-N, was used for subsequent determination of crystal structure.

Supplementary Materials: The COD entry 3000168 contains the supplementary crystallographic data for this paper. These data can be obtained free of charge via <http://www.crystallography.net/cod/search.html>. The following materials are available online at <http://www.mdpi.com/2073-4352/8/2/15/s1>.

Acknowledgments: The authors are thankful to the National Science Foundation (United States) for supporting the synthesis, characterization, and manuscript preparation (Grant DMR-1231586) of this work. A portion of this research used resources at the Spallation Neutron Source, a DOE Office of Science User Facility operated by the Oak Ridge National Laboratory. This research used resources of the Advanced Photon Source, a U.S. Department of Energy (DOE) Office of Science User Facility operated for the DOE Office of Science by Argonne National Laboratory under Contract No. DE-AC02-06CH11357. The authors wish to thank scientists and technicians working at these institutions for their help and scientific advice for this research.

Author Contributions: William R. Woerner, Alexandra Sinclair and M. Mahdi Davari Esfahani conceived and designed the experiments; William R. Woerner and M. Mahdi Davari Esfahani performed the experiments and theoretical predictions; John B. Parise, M. Mahdi Davari Esfahani, Alwin James, Artem R. Oganov, Lars Ehm and William R. Woerner analyzed the data and contributed to the text; Alwin James wrote, edited and submitted the paper.

Conflicts of Interest: The authors declare no conflict of interest.

Appendix A

Appendix A.1. Structural Description

Selected interatomic distances and angles, and bond valence sums are summarized in Table A2 and the overall structure is depicted as a polyhedral model in Figure 5. For the sake of clarity, the structure is divided into separate Ti- and Ga-rich blocks (Figure A1) with the nitrogen doped sites preferentially occupying the former structural element. The Ti-block (Figure A1) consists of four edge-shared Ti-centered octahedra, a piece of NaCl-related (TiO, TiN) structure containing the ON8 site, which is about 60% occupied by N (Table A1); this site is bonded to four Ti (Figure A1). The remainder of the block consists of edge linked Ti-octahedral chains linked to the TiN/TiO fragments at octahedral corners. With the exception of O7, all anion sites within the block, ON-1, -2, -4 and -8 are partially occupied by nitrogen.

The second block contains two symmetry independent octahedral sites, occupied mostly by Ga (Table A1) and a pure Ga-centered tetrahedral site (Figure A1).

Table A1. Final results from the joint X-ray neutron refinement of the Ga-Ti-O-N phase.

Site	Comp *	M **	x	y	z
TiGa1	0.272(7)	4	0.68066(6)	0	0.0554(1)
Ti2	1.0	4	0.48766(9)	0	0.6516(1)
TiGa3	0.245(7)	4	0.18934(6)	0	0.3871(1)
Ti4	1.0	2	0	0	0
Ga5	1.0	4	0.15770(5)	0	0.7257(1)
ON1	0.08(2)	4	0.0147(2)	0	0.2125(4)
ON2	0.08(2)	4	0.4003(2)	0	0.3039(5)
O3	1.0	4	0.1979(2)	0	0.9208(5)
ON4	0.07(2)	4	0.4277(2)	0	0.9955(4)
O5	1.0	4	0.1876(2)	0	0.1853(4)
O6	1.0	4	0.2288(2)	0	0.5998(4)
O7	1.0	4	0.3792(3)	0	0.6098(4)
ON8	0.57(1)	2	0	0	$\frac{1}{2}$

* Fractional occupancy (*f*) by Ti and N of the cation TiGa and anion ON sites, respectively; All sites were refined assuming full occupancy, e.g., $f_{\text{Ti}} + f_{\text{Ga}} = 1.0$; The chemistry was constrained so that total nitrogen in the unit cell = ((total Ti in unit cell)-6) consistent with the formulation $\text{Ti}_{6+x}\text{Ga}_{12-x}\text{O}_{30-x}\text{N}_x$. ** M = site multiplicity.

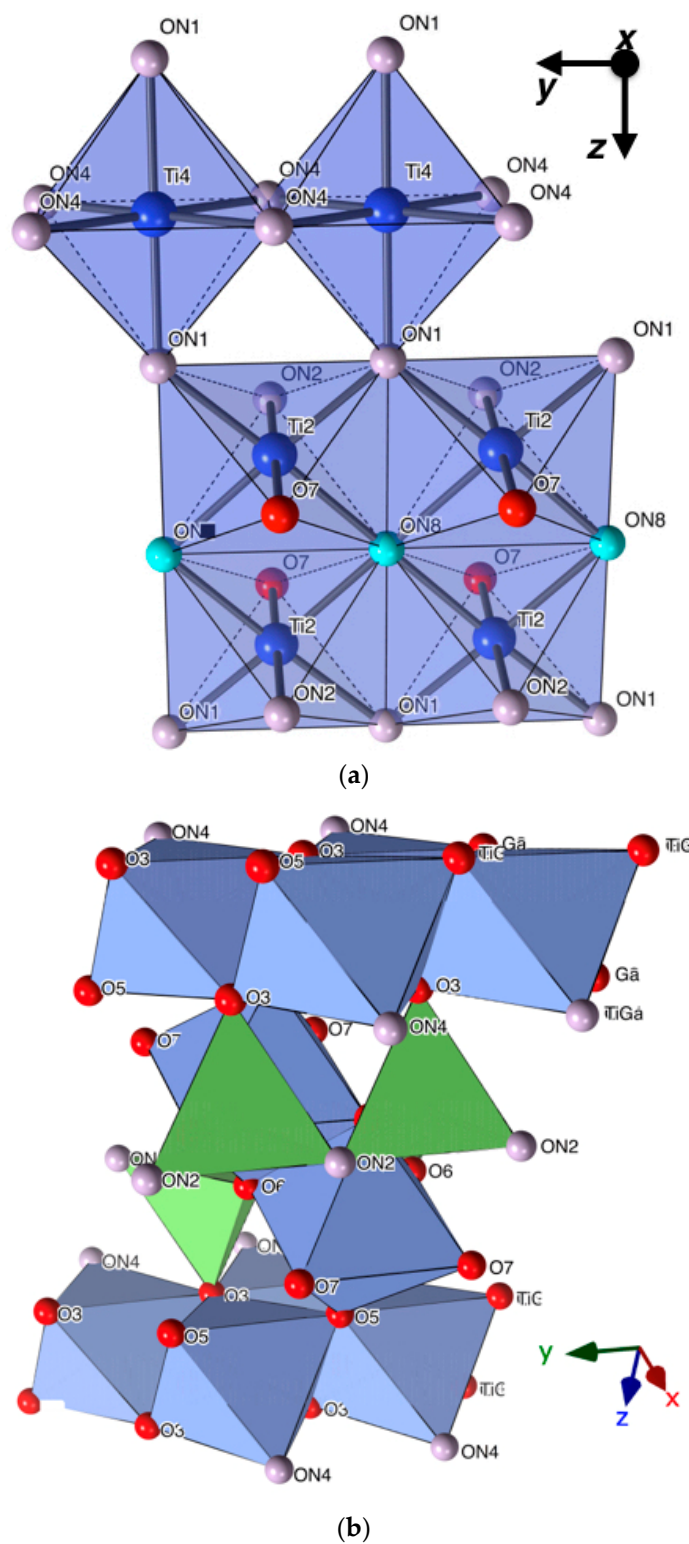


Figure A1. (a) top—Ti-block and (b) bottom—Ga-Ti block (see Figure 3).

Refined $U_{\text{iso}} \times 10^2 \text{ \AA}^2 = 0.67(1)$ and $0.41(2)$ for cation and anion sites, respectively.

Refined Composition: $\text{Ti}_8\text{Ga}_{10}\text{O}_{28}\text{N}_2$ or $\text{Ti}_4\text{Ga}_5\text{O}_{14}\text{N}$.

Unit cell: monoclinic, $C2/m$, $a = 17.823(1) \text{ \AA}$, $b = 2.9970(1) \text{ \AA}$, $c = 9.4205(5) \text{ \AA}$, $\beta = 98.446(3)^\circ$;
Volume = $497.74(3) \text{ \AA}^3$.

Refinement statistics: combined $R_{wp} = 5.57\%$ GOF = 3.69 for joint X-ray neutron data (R_{wp} = for the individual X-ray and Neutron data sets were $R^X_{wp} = 13.31\%$ (38,714 observations) and $R^N_{wp} = 2.15\%$ (4035 observations) respectively; the X-ray:neutron data were weighted 1:1.5; the integrated Bragg discrepancy factors, $R_B(F^2)$, for the Ga-Ti-O-N phase were 5.32% and 10.22%, for the X-ray and neutron data, respectively.

Table A2. Selected interatomic distances (Å) and angles (°) for the Ga-Ti-O-N phase.

TiGa1	To	dist.	$S_{ij}/\Sigma S_{ij}^*$	O3	O3	O3	ON4	O5
	O3	2.143(4)	0.43					
	O3	2.015(3)	0.58	79.7(1)				
	O3	2.015(3)	0.58	79.7(1)	96.1(2)			
	ON4	1.920(4)	0.72	171.7(2)	94.8(1)	94.8(1)		
	O5	1.927(2)	0.71	88.0(1)	79.6(1)	167.5(2)	97.3(1)	
	O5	1.927(2)	0.71	88.0(1)	167.5(2)	79.6(1)	97.3(1)	102.1(2)
			3.73					
Ti2	To	dist.		ON1	ON1	ON2	O7	ON8
	ON1	1.976(3)	0.63					
	ON1	1.976(3)	0.63	98.6(2)				
	ON2	1.980(5)	0.63	88.8(1)	88.8(1)			
	O7	1.916(5)	0.73	90.9(1)	90.9(1)	179.6(2)		
	ON8	2.104(1)	0.47	85.1(1)	174.1(1)	86.6(1)	93.6(1)	
	ON8	2.104(1)	0.47	174.1(1)	85.1(1)	86.6(1)	93.6(1)	90.86(5)
			3.57					
TiGa3	To	dist.		O5	O6	O6	O6	O7
	O5	1.897(4)	0.76					
	O6	2.025(4)	0.57	160.8(2)				
	O6	2.082(3)	0.50	88.2(1)	78.6(1)			
	O6	2.082(3)	0.50	88.2(1)	78.6(1)	92.1(2)		
	O7	1.936(3)	0.70	95.6(1)	96.5(1)	83.1(1)	173.8(2)	
	O7	1.936(3)	0.70	95.6(1)	96.5(1)	173.8(2)	83.1(1)	101.4(2)
			3.71					
Ti4	To	dist.		ON1	ON1	ON4	ON4	ON4
	ON1	1.980(4)	0.63					
	ON1	1.980(4)	0.63	180				
	ON4	1.973(3)	0.64	90.6(1)	89.4(1)			
	ON4	1.973(3)	0.64	90.6(1)	89.4(1)	98.8(2)		
	ON4	1.973(3)	0.64	89.4(1)	90.6(1)	81.2(2)	180	
	ON4	1.973(3)	0.64	89.4(1)	90.6(1)	180	81.2(2)	98.8(2)
			3.81					
Ga5	To	dist.		ON2	ON2	O3		
	ON2	1.818(3)	0.79					
	ON2	1.818(3)	0.79	111.0(2)				
	O3	1.872(4)	0.68	106.1(1)	106.1(1)			
	O6	1.859(4)	0.71	109.1(1)	109.1(1)	115.3(2)		
			2.96					

* Bond Valence $S_{ij} = \exp((R_0 - R_{ij})/B)$ where R_{ij} is the length of a bond between atoms i and j; ΣS_{ij} , the bond valence sum around each atom should be equal to the valence (oxidation state) of that atom. For the values quoted the parameters R_0 and B were taken from tabulations provided at the International Union of Crystallography: <https://www.iucr.org/resources/data/datasets/bond-valence-parameters> [48]. The R_0 and B parameters used were those compiled for Ti^{4+} (1.815, 0.37) and Ga^{3+} (1.73, 0.37) bonded to O^{2-} . TiGa sites used Ti^{4+} parameters.

Table A3. Average bond lengths of the predicted Ga-Ti-O-N structures optimized at 20 GPa.

Average Bond Lengths	GaTiO ₂ N	GaTi ₂ O ₄ N
d(Ga-ON)	1.941	1.976
d(Ti-O)	—	2.027
d(Ti-ON)	2.057	1.969

Table A4. Crystallographic Information Files (CIFs) created for GaTiO₂N and GaTiO₄N.

CIF File Created for GaTiO ₂ N							
_audit_creation_date		2017-08-05					
_symmetry_space_group_name_H-M		'PM'					
_symmetry_Int_Tables_number		6					
_symmetry_cell_setting		monoclinic					
loop_							
_symmetry_equiv_pos_as_xyz							
x,y,z							
x,-y,z							
_cell_length_a		5.9275					
_cell_length_b		3.0572					
_cell_length_c		5.2466					
_cell_angle_alpha		90.0000					
_cell_angle_beta		91.4407					
_cell_angle_gamma		90.0000					
loop_							
_atom_site_label							
_atom_site_type_symbol							
_atom_site_fract_x							
_atom_site_fract_y							
_atom_site_fract_z							
_atom_site_U_iso_or_equiv							
_atom_site_adp_type							
_atom_site_occupancy							
Ga1	Ga	0.18413	−0.00000	0.00367	0.00000	Uiso	1.00
N2	N	0.16384	−0.00000	0.37134	0.00000	Uiso	1.00
Ti1	Ti	0.50889	−0.00000	0.40778	0.00000	Uiso	1.00
O2	O	0.43639	−0.00000	0.76892	0.00000	Uiso	1.00
O4	O	0.75867	−0.00000	0.10112	0.00000	Uiso	1.00
Ga2	Ga	0.01254	0.50000	0.48200	0.00000	Uiso	1.00
N1	N	0.69627	0.50000	0.53124	0.00000	Uiso	1.00
Ti2	Ti	0.66631	0.50000	0.90342	0.00000	Uiso	1.00
O1	O	0.02938	0.50000	0.85656	0.00000	Uiso	1.00
O3	O	0.42192	0.50000	0.14854	0.00000	Uiso	1.00
CIF File Created for GaTiO ₄ N							
_audit_creation_date		2017-08-05					
_symmetry_space_group_name_H-M		'P21'					
_symmetry_Int_Tables_number		4					
_symmetry_cell_setting		monoclinic					
loop_							
_symmetry_equiv_pos_as_xyz							
x,y,z							
-x,y+1/2,-z							
_cell_length_a		4.8847					
_cell_length_b		5.0528					
_cell_length_c		6.2742					
_cell_angle_alpha		90.0000					
_cell_angle_beta		110.3545					
_cell_angle_gamma		90.0000					
loop_							
_atom_site_label							
_atom_site_type_symbol							
_atom_site_fract_x							

Table A4. Cont.

CIF File Created for GaTiO ₂ N							
_atom_site_fract_y							
_atom_site_fract_z							
_atom_site_U_iso_or_equiv							
_atom_site_adp_type							
_atom_site_occupancy							
Ga1	Ga	0.07981	0.98738	0.15399	0.00000	Uiso	1.00
N1	N	0.80267	0.11936	0.86384	0.00000	Uiso	1.00
Ti1	Ti	0.21226	0.55540	0.48175	0.00000	Uiso	1.00
Ti3	Ti	0.56276	0.49295	0.17439	0.00000	Uiso	1.00
O1	O	0.95005	0.27236	0.30543	0.00000	Uiso	1.00
O2	O	0.41028	0.91541	0.49985	0.00000	Uiso	1.00
O3	O	0.42921	0.12888	0.11294	0.00000	Uiso	1.00
O7	O	0.16559	0.28320	0.69354	0.00000	Uiso	1.00

References

- Lewis, N.S.; Nocera, D.G. Powering the planet: Chemical challenges in solar energy utilization. *Proc. Natl. Acad. Sci. USA* **2006**, *103*, 15729–15735. [[CrossRef](#)] [[PubMed](#)]
- Lewis, N.S.; Crabtree, G. *Basic Research Needs for Solar Energy Utilization: Report of the Basic Energy Sciences Workshop on Solar Energy Utilization, 18–21 April 2005*; US Department of Energy, Office of Basic Energy Science: Washington, DC, USA, 2005.
- Tsao, J.; Lewis, N.; Crabtree, G. *Solar FAQs*; US department of Energy: Washington, DC, USA, 2006; pp. 1–24.
- Hashimoto, K.; Irie, H.; Fujishima, A. TiO₂ photocatalysis: A historical overview and future prospects. *Jpn. J. Appl. Phys.* **2005**, *44*, 8269. [[CrossRef](#)]
- Fujishima, A.; Honda, K. Electrochemical photolysis of water at a semiconductor electrode. *Nature* **1972**, *238*, 37–38. [[CrossRef](#)] [[PubMed](#)]
- Fujishima, A.; Honda, K.; Kikuchi, S. Photosensitized electrolytic oxidation on semiconducting n-type TiO₂ electrode. *Kogyo Kagaku Zasshi* **1969**, *72*, 108–113. [[CrossRef](#)]
- Ruddlesden, S.N.; Popper, P. New compounds of the K₂NiF₄ type. *Acta Crystallogr.* **1957**, *10*, 538–539. [[CrossRef](#)]
- Maeda, K.; Domen, K. Oxynitride materials for solar water splitting. *MRS Bull.* **2011**, *36*, 25–31. [[CrossRef](#)]
- Fuertes, A. Synthesis and properties of functional oxynitrides—From photocatalysts to CMR materials. *Dalton Trans.* **2010**, *39*, 5942–5948. [[CrossRef](#)] [[PubMed](#)]
- Fuertes, A. Chemistry and applications of oxynitride perovskites. *J. Mater. Chem.* **2012**, *22*, 3293–3299. [[CrossRef](#)]
- Hirai, T.; Maeda, K.; Yoshida, M.; Kubota, J.; Ikeda, S.; Matsumura, M.; Domen, K. Origin of visible light absorption in GaN-rich (Ga_{1-x}Zn_x)(N_{1-x}O_x) photocatalysts. *J. Phys. Chem. C* **2007**, *111*, 18853–18855. [[CrossRef](#)]
- Kasahara, A.; Nukumizu, K.; Hitoki, G.; Takata, T.; Kondo, J.N.; Hara, M.; Kobayashi, H.; Domen, K. Photoreactions on LaTiO₂N under visible light irradiation. *J. Phys. Chem. A* **2002**, *106*, 6750–6753. [[CrossRef](#)]
- Kasahara, A.; Nukumizu, K.; Takata, T.; Kondo, J.N.; Hara, M.; Kobayashi, H.; Domen, K. LaTiO₂N as a visible-light (≤600 nm)-driven photocatalyst (2). *J. Phys. Chem. B* **2003**, *107*, 791–797. [[CrossRef](#)]
- Porter, S.H.; Huang, Z.; Dou, S.; Brown-Xu, S.; Golam Sarwar, A.T.M.; Myers, R.C.; Woodward, P.M. Electronic structure and photocatalytic water oxidation activity of RTiNO₂ (R = Ce, Pr and Nd) perovskite nitride oxides. *Chem. Mater.* **2015**, *27*, 2414–2420. [[CrossRef](#)]
- Hyett, G.; Green, M.A.; Parkin, I.P. The use of combinatorial chemical vapor deposition in the synthesis of Ti_{3-δ}O₄N with 0.06 < δ < 0.25: A titanium oxynitride phase isostructural to anosovite. *J. Am. Chem. Soc.* **2007**, *129*, 15541–15548. [[PubMed](#)]
- Hyett, G.; Green, M.A.; Parkin, I.P. Ultra-violet light activated photocatalysis in thin films of the titanium oxynitride, Ti_{3-δ}O₄N. *J. Photochem. Photobiol. A Chem.* **2009**, *203*, 199–203. [[CrossRef](#)]
- Maeda, K.; Takata, T.; Hara, M.; Saito, N.; Inoue, Y.; Kobayashi, H.; Domen, K. GaN: ZnO solid solution as a photocatalyst for visible-light-driven overall water splitting. *J. Am. Chem. Soc.* **2005**, *127*, 8286–8287. [[CrossRef](#)] [[PubMed](#)]

18. Dharmagunawardhane, H.A.N.; James, A.; Wu, Q.; Woerner, W.R.; Sinclair, A.; Palomino, R.; Orlov, A.; Parise, J.B. Unexpected visible light driven photocatalytic activity without cocatalysts and sacrificial reagents from the $(\text{GaN})_{1-x}(\text{ZnO})_x$ solid solution synthesized at high pressure in the entire composition range. *RSC Adv.* **2018**. In Review.
19. Wu, Y.B.; Lazic, P.; Hautier, G.; Persson, K.; Ceder, G. First principles high throughput screening of oxynitrides for water-splitting photocatalysts. *Energy Environ. Sci.* **2013**, *6*, 157–168. [[CrossRef](#)]
20. Woerner, W.R.; Qian, G.-R.; Oganov, A.R.; Stephens, P.W.; Dharmagunawardhane, H.N.; Sinclair, A.; Parise, J.B. Combined theoretical and in situ scattering strategies for optimized discovery and recovery of high-pressure phases: A case study of the $\text{GaN-Nb}_2\text{O}_5$ system. *Inorg. Chem.* **2016**, *55*, 3384–3392. [[CrossRef](#)] [[PubMed](#)]
21. Ozoliņš, V.; Wolverton, C.; Zunger, A. First-principles theory of vibrational effects on the phase stability of Cu-Au compounds and alloys. *Phys. Rev. B* **1998**, *58*, R5897. [[CrossRef](#)]
22. Vinograd, V.L. Substitution of $^{[4]}\text{Al}$ in layer silicates: Calculation of the Al-Si configurational entropy according to ^{29}Si NMR spectra. *Phys. Chem. Miner.* **1995**, *22*, 87–98. [[CrossRef](#)]
23. Brown, I.D.; Altermatt, D. Bond-valence parameters obtained from a systematic analysis of the inorganic crystal structure database. *Acta Crystallogr. Sect. B* **1985**, *41*, 244–247. [[CrossRef](#)]
24. Lüdtke, T.; Orthmann, S.; Lerch, M. Bixbyite-type phases in the system Ta-Zr-ON. *Z. Naturforsch. B* **2017**, *72*, 305–311. [[CrossRef](#)]
25. Kuno, Y.; Tassel, C.; Fujita, K.; Batuk, D.; Abakumov, A.M.; Shitara, K.; Kuwabara, A.; Moriwake, H.; Watabe, D.; Ritter, C. ZnTaO_2N : Stabilized high-temperature LiNbO_3 -type structure. *J. Am. Chem. Soc.* **2016**, *138*, 15950–15955. [[CrossRef](#)] [[PubMed](#)]
26. Oró-Solé, J.; Clark, L.; Bonin, W.; Attfield, J.P.; Fuertes, A. Anion-ordered chains in ad 1 perovskite oxynitride: NdVO_2N . *Chem. Commun.* **2013**, *49*, 2430–2432. [[CrossRef](#)] [[PubMed](#)]
27. Yashima, M.; Lee, Y.; Domen, K. Crystal structure and electron density of Tantalum oxynitride, a visible light responsive photocatalyst. *Chem. Mater.* **2007**, *19*, 588–593. [[CrossRef](#)]
28. Srinivasa, S.; Cartz, L.; Jorgensen, J.; Worlton, T.; Beyerlein, R.; Billy, M. High-pressure neutron diffraction study of $\text{Si}_2\text{N}_2\text{O}$. *J. Appl. Crystallogr.* **1977**, *10*, 167–171. [[CrossRef](#)]
29. Momma, K.; Izumi, F. Vesta: A three-dimensional visualization system for electronic and structural analysis. *J. Appl. Crystallogr.* **2008**, *41*, 653–658. [[CrossRef](#)]
30. Cros, B.; Kernerczeskleba, H.; Philippot, E. The structure of V_2GaO_5 . *Acta Crystallogr. Sect. B-Struct. Commun.* **1980**, *36*, 2210–2213. [[CrossRef](#)]
31. Suchomel, M.R.; Ribaud, L.; Von Dreele, R.B.; Toby, B.H. Synchrotron powder diffraction simplified: The high-resolution diffractometer 11-BM at the Advanced Photon Source. *Geochim. Cosmochim. Acta* **2010**, *74*, 12.
32. Wang, J.; Toby, B.H.; Lee, P.L.; Ribaud, L.; Antao, S.M.; Kurtz, C.; Ramanathan, M.; Von Dreele, R.B.; Beno, M.A. A dedicated powder diffraction beamline at the advanced photon source: Commissioning and early operational results. *Rev. Sci. Instrum.* **2008**, *79*, 085105. [[CrossRef](#)] [[PubMed](#)]
33. Toby, B.H.; Huang, Y.; Dohan, D.; Carroll, D.; Jiao, X.S.; Ribaud, L.; Doebbler, J.A.; Suchomel, M.R.; Wang, J.; Preissner, C.; et al. Management of metadata and automation for mail-in measurements with the aps 11-BM high-throughput, high-resolution synchrotron powder diffractometer. *J. Appl. Crystallogr.* **2009**, *42*, 990–993. [[CrossRef](#)]
34. Toby, B.H.; Von Dreele, R.B. GSAS-II: The genesis of a modern open-source all purpose crystallography software package. *J. Appl. Crystallogr.* **2013**, *46*, 544–549. [[CrossRef](#)]
35. Stephens, P.W. Phenomenological model of anisotropic peak broadening in powder diffraction. *J. Appl. Crystallogr.* **1999**, *32*, 281–289. [[CrossRef](#)]
36. Balzar, D.; Audebrand, N.; Daymond, M.R.; Fitch, A.; Hewat, A.; Langford, J.I.; Le Bail, A.; Louer, D.; Masson, O.; McCowan, C.N.; et al. Size-strain line-broadening analysis of the Ceria round-robin sample. *J. Appl. Crystallogr.* **2004**, *37*, 911–924. [[CrossRef](#)]
37. Ha, K.; Ciria, M.; O’Handley, R.C.; Stephens, P.W.; Pagola, S. X-ray study of strains and dislocation density in epitaxial Cu/Ni/Cu/Si(001) films. *Phys. Rev. B* **1999**, *60*, 13780–13785. [[CrossRef](#)]
38. Brese, N.E.; O’Keeffe, M.; Rauch, P.; DiSalvo, F.J. Structure of Ta_3N_5 at 16 K by time-of-flight neutron diffraction. *Acta Crystallogr. C* **1991**, *47*, 2291–2294. [[CrossRef](#)]

39. Glass, C.W.; Oganov, A.R.; Hansen, N. USPEX—Evolutionary crystal structure prediction. *Comput. Phys. Commun.* **2006**, *175*, 713–720. [[CrossRef](#)]
40. Lyakhov, A.O.; Oganov, A.R.; Stokes, H.T.; Zhu, Q. New developments in evolutionary structure prediction algorithm USPEX. *Comput. Phys. Commun.* **2013**, *184*, 1172–1182. [[CrossRef](#)]
41. Lyakhov, A.O.; Oganov, A.R.; Valle, M. How to predict very large and complex crystal structures. *Comput. Phys. Commun.* **2010**, *181*, 1623–1632. [[CrossRef](#)]
42. Oganov, A.R.; Glass, C.W. Evolutionary crystal structure prediction as a tool in materials design. *J. Phys. Condens. Matter* **2008**, *20*, 064210. [[CrossRef](#)] [[PubMed](#)]
43. Oganov, A.R.; Lyakhov, A.O.; Valle, M. How evolutionary crystal structure prediction works and why. *Acc. Chem. Res.* **2011**, *44*, 227–237. [[CrossRef](#)] [[PubMed](#)]
44. Blöchl, P.E. Projector augmented-wave method. *Phys. Rev. B* **1994**, *50*, 17953. [[CrossRef](#)]
45. Kresse, G.; Furthmüller, J. Efficient iterative schemes for ab initio total-energy calculations using a plane-wave basis set. *Phys. Rev. B* **1996**, *54*, 11169. [[CrossRef](#)]
46. Perdew, J.P.; Burke, K.; Ernzerhof, M. Generalized gradient approximation made simple. *Phys. Rev. Lett.* **1996**, *77*, 3865. [[CrossRef](#)] [[PubMed](#)]
47. Monkhorst, H.J.; Pack, J.D. Special points for brillouin-zone integrations. *Phys. Rev. B* **1976**, *13*, 5188. [[CrossRef](#)]
48. Brown, I.D. *The Chemical Bond in Inorganic Chemistry: The Bond Valence Model*; Oxford University Press: Oxford, UK, 2002.



© 2018 by the authors. Licensee MDPI, Basel, Switzerland. This article is an open access article distributed under the terms and conditions of the Creative Commons Attribution (CC BY) license (<http://creativecommons.org/licenses/by/4.0/>).